Available online at www.sciencedirect.com
ScienceDirect
International Journal of Heat and Mass Transfer 51 (2008) 1034–1048
International Journal of HEAT and MASS TRANSFER
www.elsevier.com/locate/ijhmt

Mixed convection from an isolated spherical particle

S. Bhattacharyya *, A. Singh

Department of Mathematics, Indian Institute of Technology, Kharagpur 721 302, India

Received 3 May 2007; received in revised form 21 May 2007
Available online 19 December 2007

Abstract

A numerical study on mixed convection around a hot spherical particle moving vertically downwards in a still fluid medium has been made. The flow field is considered to be axisymmetric for the range of Reynolds number (based on the diameter and the settling velocity of the particle) considered. A third-order accurate upwind scheme is employed to compute the flow field and the temperature distribution. The form of the wake and the thermal field is analyzed for several values of Grashof number and the Reynolds number. The influence of buoyancy on drag and the rate of heat transfer are studied. At moderate Reynolds number, recirculating eddy develops in the downstream of the sphere. With the rise of surface temperature this eddy collapses and the fluid adjacent to the heated surface develops into a buoyant plume above the sphere. The increase in surface temperature of the sphere delays the flow separation. Our results show that the drag force and the rate of heat transfer strongly depend on Grashof number for the moderate values of Reynolds number. The conjugate heat transfer from the moving sphere is also addressed in the present paper. We have compared our computed solution with several empirical and asymptotic expressions available in the literature and found them in good agreement.

Keywords: Heat transfer; Thermal plume; Buoyancy; Upwind scheme; Separation

1. Introduction

The dynamics of solid particles submerged in a fluid medium is of interest in many engineering processes, such as vaporization and condensation of fuel droplets, manufacturing systems, fuel spray, coal combustion and motion of aerosol particles. The hydrodynamic interaction between suspended particles and the surrounding fluid phase is of interest also in colloid, polymer, aerosol and physiological systems. Over the years, several studies have been made on flow past particles of various shapes, such as rigid sphere, spheroids, and cylinders. A wide variety of numerical and analytical methods have been used to obtain solutions for a broad range of geometric and flow parameters. Most of the earlier studies have been included in the books by Happel and Brenner [1] and Clift et al. [2]. Recent works on numerical and experimental studies on spherical particles falling in unconfined fluids is discussed in Michaelides [3]. Several authors have used the finite element/ finite volume method for direct numerical simulation of particles sedimentation in 2D and 3D [4,5]. The particle–fluid interaction problems with high number of particles are complicated owing to the necessity of geometrically adapted grid generation. The lattice Boltzmann method (LBM) to simulate the particulate motion have proven to be more efficient in recent years. A detailed discussions on recent models using LBM have been made by Feng and Michaelides [6]. In this paper, however, we restricted our discussion on the motion due to a single particle.

The fluid flow past a stationary isolated sphere at varying Reynolds number has been considered by several authors experimentally and/or numerically because of its complex nature. The dye visualization study of Magavey and Bishop [7] reveals that sphere wake remains steady symmetric up to Reynolds number 210. Their results show that the transition from a steady axisymmetric with a

* Corresponding author.
E-mail address: somnath@maths.iitkgp.ernet.in (S. Bhattacharyya).

0017-9310/$ - see front matter © 2007 Elsevier Ltd. All rights reserved.
doi:10.1016/j.ijheatmasstransfer.2007.05.033

Nomenclature

C_d	drag coefficient, $F_d/\frac{1}{2}\rho U_\infty^2 \pi R^2$
c_p	specific heat
C_p	pressure coefficient, $(p^* - p_\infty)/\frac{1}{2}\rho U_\infty^2$
g	gravitational acceleration
Gr	Grashof number, $4g\beta(T_s - T_\infty)R^3/v^2$
$\overline{Nu}$	total Nusselt number
Nu	local Nusselt number
Pe	Peclet number, $2U_\infty R/\alpha$
Pr	Prandtl number, v/α
r	dimensionless radial coordinate
R	sphere radius
Re	Reynolds number, $2U_\infty R/v$
Ri	Richardson number, Gr/Re^2
t	dimensionless time
T	dimensionless temperature
u	dimensionless radial velocity
U_∞	free stream velocity
v	dimensionless cross-radial velocity

Greek symbols

α	thermal diffusivity, $\kappa/\rho c_p$
α_e	thermal diffusivity of the solid sphere
β	coefficient of thermal expansion, $-(\frac{\delta\rho}{\delta T})_p/\rho_\infty$
κ	thermal conductivity
μ	dynamic viscosity
v	kinematic viscosity, μ/ρ
ρ	fluid density
θ	angular coordinate
ψ	non-dimensional stream function
ζ	non-dimensional vorticity

Subscripts

e	inside of the sphere
s	surface of the sphere
∞	free stream

Superscript

*	dimensional quantity

attached separation bubble to a steady non-axisymmetric wake consisting of a shortened separation bubble with two trailing counter-rotating vortices occurs at approximately at $Re = 211$. Subsequently, Johnson and Patel [8], Tomboulides and Orszag [9] and Thomson et al. [10] found that the sphere wake experiences a transition to a steady asymmetric wake from a steady axisymmetric wake at a Reynolds number which lies in the range 210–220. As Reynolds number increases above 270, the flow is three-dimensional and time-dependent with periodic vortex shedding [11,12]. Bagchi et al. [12] studied the vortex shedding phenomena and its effect on heat transfer from a sphere. Yun et al. [13] studied the vortical structure behind a sphere at a subcritical Reynolds number. From those studies it may be noted that vortex shedding has a difference in characteristics from that of a circular cylinder. The vortex shedding from a circular cylinder occurs for Reynolds number above 40. In case of a circular cylinder, shedding of vortices occurs from either side of the cylinder where as, vortices are shed only from the top of the sphere.

Heat transfer from or to a body of spherical or near spherical shape is a problem of great practical importance. Acrivos and Taylor [14], Bernner [15], and Dennis et al. [16] investigated the heat and mass transfer from spherical and arbitrary shaped bodies at small Peclet numbers in forced convection dominated regime. In a recent article by Feng and Michaelides [17] and in the book by Michaelides [3] provided a detail account on recent advances on the analytical form of the hydrodynamic force and heat transfer from spherical particles in slow motion. The steady state natural convection over a sphere has been studied numerically by Jia and Gogos [18] for a wide range of Grashof numbers and who have also made a discussion on some of the previous work. Their results show that a steady state buoyancy plume with a mushroom-shaped front forms above the sphere whose length and thickness decrease with increasing Grashof number. Recently, Yang et al. [19] studied a similar natural convection problem for a wider range of Grashof number and Prandtl number.

The convection of heated drops and particles through a fluid medium induces a disturbance to the host fluid due to the buoyant force. The mixed convection about a point heat source is made by Riely and Darke [20] through a boundary-layer analysis. Subsequently, Riely and Tveitereid [21] made the linear stability analysis due to an axisymmetric buoyant plume above a point heat source in presence of a co-flowing vertical stream. Their analysis shows that the forced flow has a stabilizing effect. The local vorticity and the local potential energy in the plume are reduced by the introduction of the external stream. The sedimentation of solid particles in a hotter or colder fluid within a vertical channel is studied by Gan et al. [22]. They made a two-dimensional study with particles represented as circles. Due to the two-dimensional simulation, vortex shedding sets-in and wake becomes oscillatory at a much lower Reynolds number as compared to the case where the particles are considered to be spherical.

The combined convection due to a solid sphere has been studied by Nguyen et al. [23] for different values of Reynolds number and Grashof number. There the authors provided a discussion on some of the related studies based on either boundary layer solution or solution of two-dimensional Navier–Stokes equations. However, their study did not provide a detailed analysis on the wake characteristics and its influence on the heat transfer form the sphere for a wider range of flow parameters. The experimental studies

on the forces experienced by a heated sphere in mixed convection either due to a cross-flow or vertical flows are reported in the papers by Ziskind et al. [24] and Mograbi et al. [25] for small values of Reynolds number and Grashof number. Mograbi and Bar-Ziv [26,27] presented a combined numerical and experimental study on steady state mixed convection around a small spherical particle in the diameter range of 10–200 for small values of Reynolds, 0–0.3, and Grashof number in the range 0–0.1. They considered both buoyancy aided and opposed flows and proposed a qualitative expression for the drag force induced on the particle for low Reynolds number and Grashof number.

In most practical applications on the dynamics of heated spherical particles, the Reynolds number and Grashof number are small but finite. The analysis based on low Reynolds number and Peclet number may not be valid in many practical cases. Besides, most of the earlier studies on natural and mixed convection, as discussed above, concentrated on the heat transfer and the forces experienced by the particle. The form of the wake and the dependence of drag and heat transfer on flow parameters in mixed convection regime have not been analyzed in details. The particulate matter actively participates in defining the surrounding flow, which has not been discussed in details in all the previous studies discussed before.

In this paper, we studied the mixed convection from a heated sphere for low to moderate range of Reynolds number ($1 \leqslant Re \leqslant 200$) and Grashof number ($0 \leqslant Gr \leqslant 6 \times 10^4$). The influence of buoyancy on heat transfer and the form of the wake has been investigated. Flow field and heat transfer is analyzed for different values of the Richardson number ($Ri = Gr/Re^2$). We investigated the mechanism of the vortex collapse and subsequent generation of thermal plume in the near wake. We also considered the case where the internal thermal field of the sphere is described through a conjugate model and compared our results with Nguyen et al. [23].

In the present analysis the Reynolds number is considered to be below 200, so that the flow may be assumed to be steady, axisymmetric. Several studies on heated cylinder exposed to a vertical upward jet reported the breakdown of vortex shedding and formation of a steady wake by heating the cylinder [28,29]. From the previous literature discussions we found that the first transition from steady axisymmetry to steady non-axisymmetry occurs for Re at 200. Thus it is expected that the heat input to the sphere may extend the limit of Reynolds number for which a steady non-axisymmetry develops. Further, the collapse of vortex through increase of heat, as observed in our study, justifies the axisymmetric assumption.

2. Mathematical formulation

The flow configuration is shown in Fig. 1. A sphere of radius R heated to a constant temperature T_s (for isothermal case) is considered to be fixed in a vertically upward (anti-parallel with the gravitational acceleration) uniform stream U_∞ with ambient fluid temperature T_∞ ($<T_s$). The positive z-direction is taken as the direction of the external velocity. We consider the spherical polar coordinate (r, θ, ϕ) with the origin fixed at the center and $\theta = 0$ line along the positive z-direction. The characteristic length is taken to be R, velocity field is scaled by U_∞, the pressure by $\frac{1}{2}\rho U_\infty^2$ and the gravitational acceleration by its magnitude g. The flow field is considered to be axisymmetric with z-axis as the axis of symmetry. Introducing the stream function ψ as

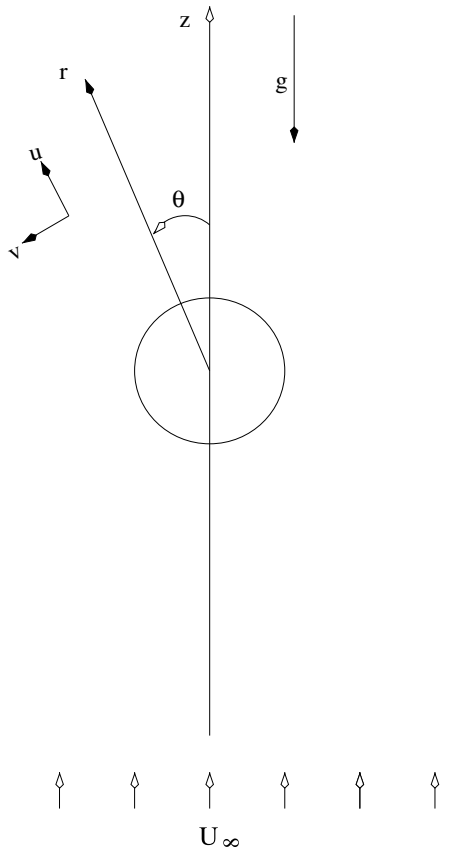

Fig. 1. Flow configuration.

$$u = \frac{1}{r^2 \sin\theta}\frac{\partial \psi}{\partial \theta}, \quad v = -\frac{1}{r \sin\theta}\frac{\partial \psi}{\partial r}. \tag{1}$$

The azimuthal vorticity component ζ can be expressed as

$$\zeta = \frac{\partial v}{\partial r} + \frac{v}{r} - \frac{1}{r}\frac{\partial u}{\partial \theta}. \tag{2}$$

Thus, the vorticity stream function relation is given by

$$\begin{aligned} E^2\psi &= -\Omega, \\ \Omega &= \zeta r \sin\theta. \end{aligned} \tag{3}$$

The non-dimensional vorticity transport equation and the energy equation with the Boussinesq approximation can be expressed as

$$\frac{\partial \Omega}{\partial t}+\frac{1}{r^2\sin\theta}\left(\frac{\partial \psi}{\partial \theta}\frac{\partial \Omega}{\partial r}-\frac{\partial \psi}{\partial r}\frac{\partial \Omega}{\partial \theta}\right)+\frac{2\Omega}{r^2\sin^2\theta}\left(\cos\theta\frac{\partial \psi}{\partial r}-\frac{\sin\theta}{r}\frac{\partial \psi}{\partial \theta}\right)=\frac{2}{Re}E^2\Omega-\frac{Gr}{Re^2}\left(r\sin\theta\frac{\partial T}{\partial r}+\cos\theta\frac{\partial T}{\partial \theta}\right)\sin\theta, \tag{4}$$

$$\frac{\partial T}{\partial t}+\frac{1}{r^2\sin\theta}\left(\frac{\partial \psi}{\partial \theta}\frac{\partial T}{\partial r}-\frac{\partial \psi}{\partial r}\frac{\partial T}{\partial \theta}\right)=\frac{2}{PrRe}\nabla^2 T. \tag{5}$$

The last term in the vorticity transport equation (4) is due to the buoyancy. The viscous dissipation has been neglected in the energy equation (5). Here

$$E^2=\frac{\partial^2}{\partial r^2}+\frac{1}{r^2}\frac{\partial^2}{\partial \theta^2}-\frac{\cot\theta}{r^2}\frac{\partial}{\partial \theta},$$

$$\nabla^2=\frac{\partial^2}{\partial r^2}+\frac{1}{r^2}\frac{\partial^2}{\partial \theta^2}+\frac{2}{r}\frac{\partial}{\partial r}+\frac{\cot\theta}{r^2}\frac{\partial}{\partial \theta}.$$

For non-isothermal case, the internal temperature field of the sphere is governed by the following equation:

$$\frac{\partial T_e}{\partial t_e}=\nabla^2 T_e. \tag{6}$$

The variables are non-dimensionalized as follows:

$$r=\frac{r^*}{R},\quad u=\frac{u^*}{U_\infty},\quad v=\frac{v^*}{U_\infty},\quad t=\frac{t^*U_\infty}{R},$$

$$\Omega=\frac{\Omega^*}{U_\infty},\quad \psi=\frac{\psi^*}{U_\infty R^2},\quad \zeta=\frac{\zeta^* R}{U_\infty},\quad T=\frac{T^*-T_\infty}{T_s-T_\infty}$$

where an asterisk has been used to indicate dimensional quantities. In accordance with the Nguyen et al. [23], we take the time scale inside the sphere as $t_e=t^*\alpha_e/R^2$. The two time scales are related by $t=(Pe/\phi_\alpha)t_e$, where ϕ_α is the ratio between the effective diffusivity of the fluid and solid.

The above governing equations are subjected to the following boundary conditions.

On the surface of sphere

$$\psi=0,\quad T=1,\quad \Omega=-\frac{\partial^2\Psi}{\partial r^2},\quad r=1,\quad 0\leqslant\theta\leqslant\pi. \tag{7}$$

Along the axis of symmetry

$$\psi=0,\quad \frac{\partial T}{\partial \theta}=0,\quad \Omega=0,\quad r>1,\quad \theta=0,\pi. \tag{8}$$

Along the for field

$$\psi=\frac{1}{2}r^2\sin^2\theta,\quad T=0,\quad \Omega=0,\quad r\to\infty,\quad 0\leqslant\theta\leqslant\pi. \tag{9}$$

The internal temperature T_e for the conjugate problem is considered to assume a finite value at the center of the sphere and the temperature at the surface of the sphere satisfies the following continuity of temperature and heat flux conditions:

$$T(t,1,\theta)=T_e(t_e,1,\theta),\quad \frac{\partial T(t,1,\theta)}{\partial r}=\phi_\kappa\frac{\partial T_e(t_e,1,\theta)}{\partial r}. \tag{10}$$

Here ϕ_κ is the ratio between the heat transfer coefficient due to fluid and solid. The flow is assumed to start impulsively from rest. Thus at $t=0$ we assumed $\psi=\zeta=T=0$ and $T_e=1$ inside the computational domain.

3. Numerical method

A fractional step method, the alternating-direction-implicit scheme (ADI), has been used for temporal discretization of the vorticity transport equation (4) and the energy equation (5). At every fractional time step the Poisson equation (3) for stream function is solved iteratively using the successive over relaxation (SOR) technique. In order to linearize the non-linear system of differential equations, a quasi-linearization approximation has been employed. At every time step, we approximate the non-linear term as

$$\left(v\frac{\partial \Omega}{\partial \theta}\right)^{k+1}=v^k\left(\frac{\partial \Omega}{\partial \theta}\right)^{k+1}$$

with $k\geqslant 0$, is the iteration index. At the start of the iteration the coefficients of the derivative are evaluated from the previous time step solution. The spatial derivatives in the vorticity transport, and energy equation are discretized through the following third-order accurate upwind scheme:

$$v_{i,j}\left(\frac{\partial \Omega}{\partial \theta}\right)=v_{i,j}(\Omega_{i+2,j}-2\Omega_{i+1,j}+9\Omega_{i,j}-10\Omega_{i-1,j}+2\Omega_{i-2,j})/(6\delta\theta)\quad \text{for } v_{i,j} \text{ positive}$$

$$v_{i,j}\left(\frac{\partial \Omega}{\partial \theta}\right)=v_{i,j}(-2\Omega_{i+2,j}+10\Omega_{i+1,j}-9\Omega_{i,j}+2\Omega_{i-1,j}-\Omega_{i-2,j})/(6\delta\theta)\quad \text{for } v_{i,j} \text{ negative}$$

with $i=3,\ldots,M-2$ and $j=3,\ldots,N-2$ where $M\times N$ are the total grid positions. The diffusion term are discretized through a second-order accurate central difference scheme:

$$(\Omega_{\theta\theta})_{i,j}=(\Omega_{i-1,j}-2\Omega_{i,j}+\Omega_{i+1,j})/\delta\theta^2,$$

$$(\Omega_{rr})_{i,j}=(\Omega_{i,j-1}-2\Omega_{i,j}+\Omega_{i,j+1})/\delta r^2.$$

But at $i=2$ or $M-1$ and $j=2$ or $N-1$ this formula is not applicable. In this case we have used a central difference formula i.e.,

$$(\Omega_\theta)_{i,j}=(\Omega_{i+1,j}-\Omega_{i-1,j})/2\delta\theta,$$

$$(\Omega_r)_{i,j}=(\Omega_{i,j+1}-\Omega_{i,j-1})/2\delta r.$$

A series of test runs were made for determining the optimal grid size and the runs were performed with various grid sizes for two different lengths of outer boundary (L_d). The outer boundary is chosen large enough so that the influence of the boundary condition on the wall shear stress and local Nusselt number are negligible. Fig. 2a and b shows

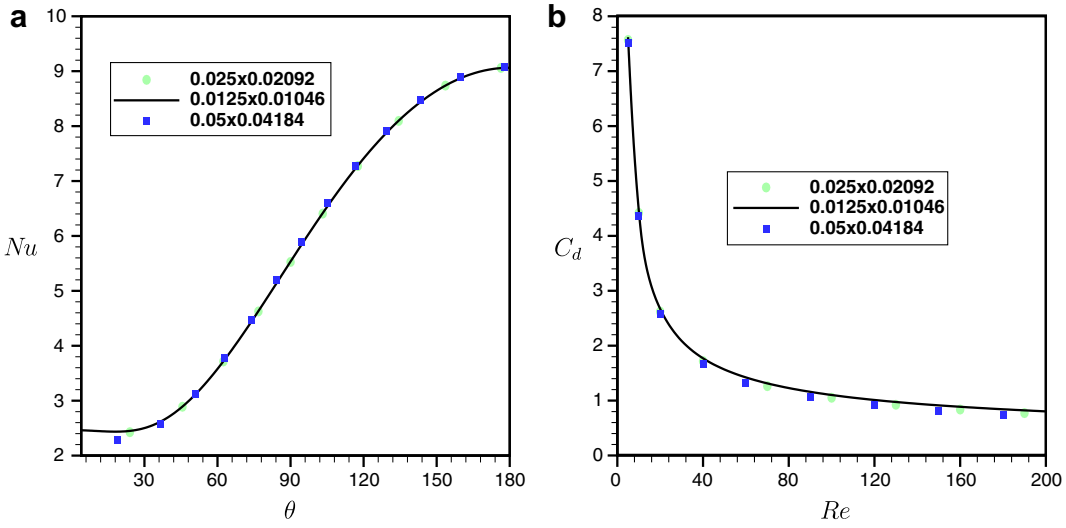

Fig. 2. Grid size effects on local Nusselt number and drag coefficient for $Re = 50$ and $Ri = 0$. (a) Nu; (b) C_d.

the grid size effect at $Re = 50$ on the local Nusselt number distribution and drag coefficient. The code was tested for three different grid sizes, namely 0.025×0.02092, 0.0125×0.01046 and 0.05×0.04184, with the first and second number being the grid size in the radial and in the cross-radial direction, respectively. By halving the grid size from 0.025×0.02092 to 0.0125×0.01046 our result (Fig. 2a and b) shows that the change in Nu and C_d is almost insignificant. Thus, we find that the grid size 0.0125×0.01046 is optimal.

To validate the present algorithm, we have compared our results for forced convection ($Ri = 0$) due to an isothermal sphere with the results due to Chang and Maxey [30] and Bagchi et al. [12]. Fig. 3a and b displays the comparison of the surface pressure and surface vorticity distribution at different Re with the results due to Chang and Maxey [30]. Fig. 4 shows the comparison of the drag coefficient and the total Nusselt number for $10 \leqslant Re \leqslant 200$ with Bagchi et al. [12] for the case of forced convection ($Ri = 0$). We have compared our results for C_d and $\overline{Nu}$ for the case of forced convection ($Ri = 0$) with the empirical formula provided by Feng and Michaelides [6] in Fig. 4. Comparisons of total Nusselt number and drag are also made with Jia and Gogos [18] for the case of natural convection at different values of Grashof number (see Fig. 5a and b). It is clear from Figs. 3–5 that our results are in total agreement with all those published results. We made a comparison of our mixed convection results for the conjugate heat transfer case with those of Nguyen et al. [23] for different values of Reynolds number and Grashof number. Fig. 6a–c shows the comparison of surface pressure, vorticity and average rate of heat transfer from the sphere for

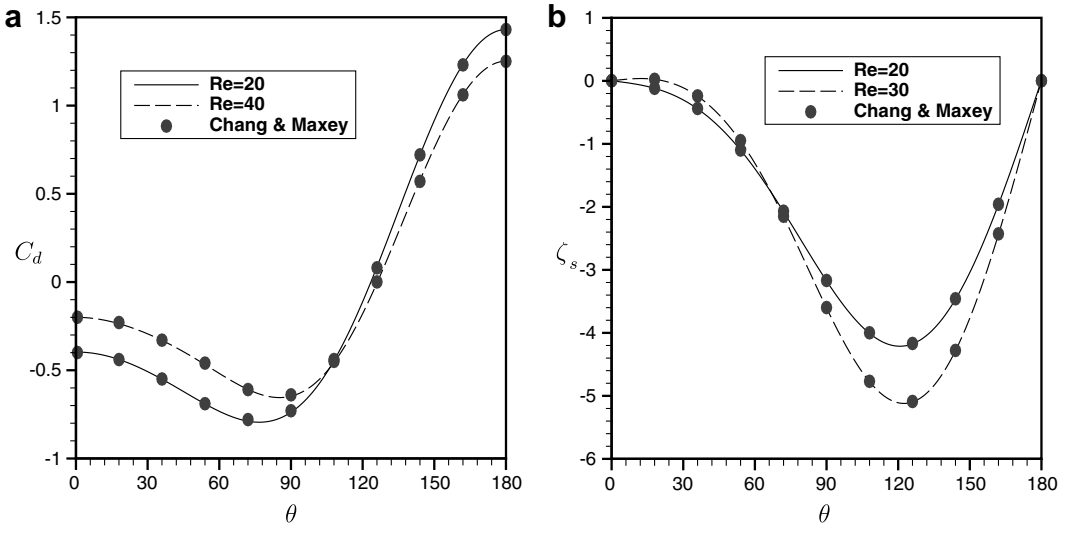

Fig. 3. Comparison of our results for forced convection ($Ri = 0$) at different Re with Chang and Maxey [30]. (a) Surface pressure (C_p); (b) surface vorticity (ζ_s) when $Ri = 0$.

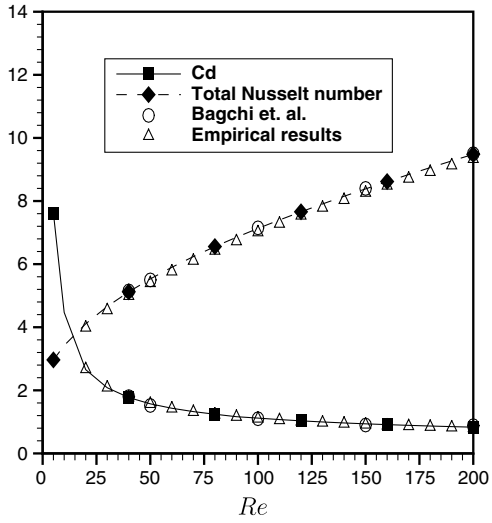

Fig. 4. Comparison of our results for drag coefficient (C_d) and total Nusselt number ($\overline{Nu}$) for forced convection ($Ri = 0$) at different Re with Bagchi et al. [12].

$Re = 80$ and $Pr = 0.7$ at different values of Grashof number namely, $Gr = 10^5, 0, 10^{-5}$. Our results are in total agreement with the results due to Nguyen et al. [23]. We have computed the Nusselt number for conjugate heat transfer case and compared with the asymptotic solution [34] and computed solutions of Nguyen et al. [23] at different Reynolds number and Peclet number. A detailed discussion on this is made in next section (Fig. 18a and b).

4. Results and discussion

We have computed the flow field for low to moderate range of Reynolds number, $1 \leqslant Re \leqslant 200$, at different values of Grashof number ($0 \leqslant Gr \leqslant 6 \times 10^4$) such that the Richardson number, Ri assumes values greater than one as well as less than one. The Richardson number measures the relative importance of the forced and buoyant effects. The Prandtl number is taken to be 0.72 for all calculation. In order to check the time dependency of the flow field we present the time evolution of the total Nusselt number distribution at different values of the flow parameters, namely $Re = 200$ and $Ri = 0$,0.5 and 1.5. The results show (Fig. 7) that the total Nusselt number distribution becomes steady after a short transition.

The streamlines and vorticity contours at different Reynolds number and Richardson number is presented in Figs. 8 and 9. We found that the flow separation occurs for $Re > 20$, when the buoyancy is not considered ($Gr = 0$). The size of the recirculation zone increases with the increase of Reynolds number. The effect of heat input to the sphere causes the low-density fluid close to the surface to move upwards, which results in a strong upward jet along the downstream side of the sphere. This buoyancy induced upward jet prevents the development of back flow as is seen for $Ri = 0$ case. The heated fluid is realigned upward and rises in a steady axisymmetric buoyant plume. Fig. 8c shows that the strength of the upward jet increases as the surface temperature is increased. The collapse of rear vortex due to density stratification was observed by Torres et al. [31].

The vorticity contour at different Reynolds number, $Re = 1, 150, 200$ is presented in Fig. 9a–c at different Ri (=0, 0.5, 1.5). We find that the strength of the vorticity close to the surface increases with the rise of surface temperature. The thickness of the boundary layer reduces as the sphere temperature is increased. In the buoyancy induced flow, the vorticity is also generated through the thermally induced baroclinic vorticity production governed by the last term in the right-hand side of the vorticity transport equation (4). We find that the input of heat to the sphere causes a narrower wake of the sphere.

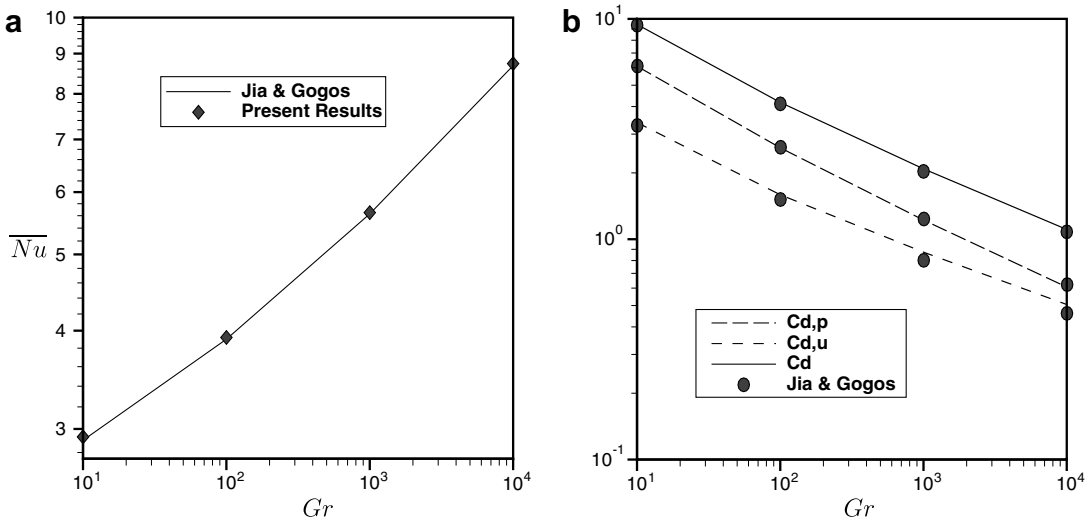

Fig. 5. Comparison of our results for total Nusselt number, drag due to pressure, drag due to viscous force and total drag coefficient in natural convection with the results due to Jia and Gogos [18] at $Pr = 0.72$ and different Gr. (a) Total Nusselt number ($\overline{Nu}$); (b) total drag (C_d), pressure drag ($C_{d,p}$) and viscous drag ($C_{d,\mu}$).

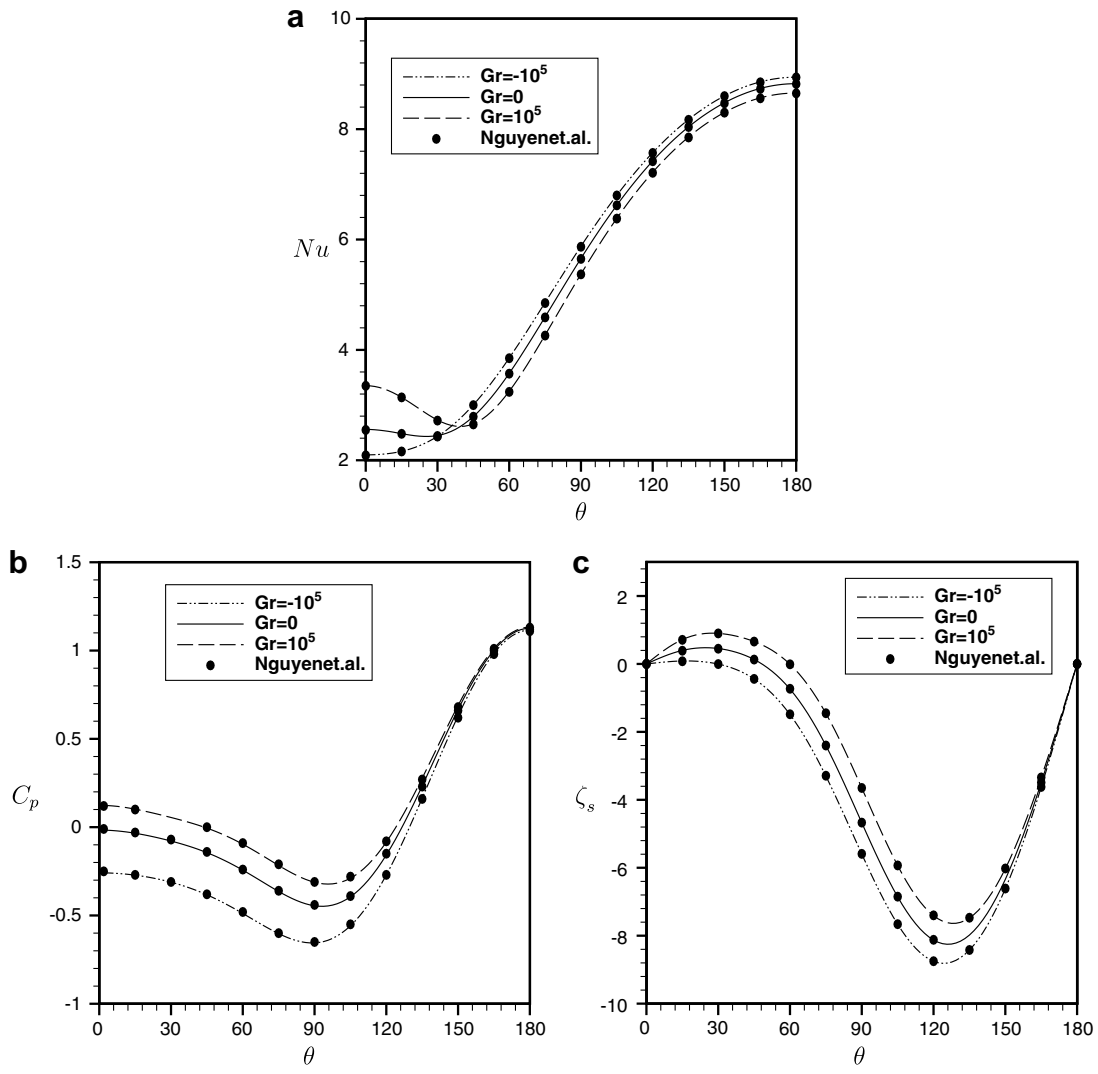

Fig. 6. Comparison of our results for conjugate case when $Re = 80$ at different Gr with $\phi_\alpha = 0.005$ and $\phi_\kappa = 1.333$ with Nguyen et al. [23]. (a) Local Nusselt number (Nu); (b) surface pressure C_p; (c) surface vorticity ζ_s.

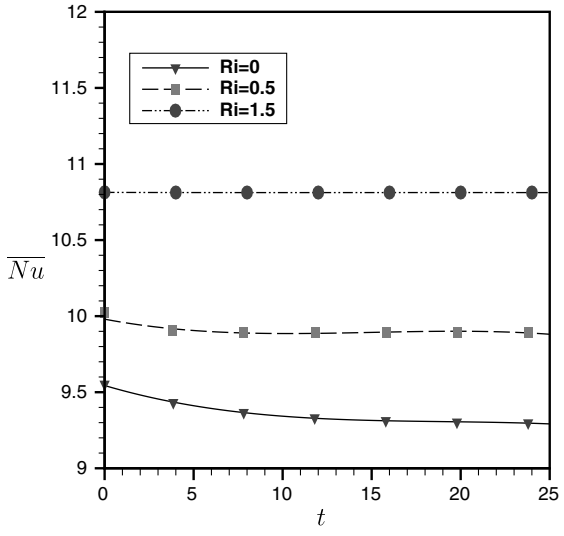

Fig. 7. Time evolution of the total Nusselt number ($\overline{Nu}$) at $Re = 200$ for different Ri (=0, 0.5, 1.5).

The surface vorticity ζ_s at different Richardson number (=0, 0.5, 1.5) is plotted in Fig. 10 at $Re = 200$. The occurrence of flow separation for $Ri = 0$ is evident from the figure. For steady axisymmetric flow, the change in sign of wall vorticity signifies the separation. The separation point shifts towards the rear stagnation point as Ri increases. At $Re = 200$ and $Ri = 1.5$ ($Gr = 6 \times 10^4$), flow does not separate. The thickness of the boundary layer reduces with the rise of surface temperature.

The surface pressure distribution C_p is presented in Fig. 11a and b. The pressure coefficients are positive in the upstream face of the sphere, and negative in the downstream side. The pressure coefficient is close to one, the inviscid value, at the forward stagnation point ($\theta = \pi$) at the Reynolds number 100. The forward stagnation point pressure deviates from one for lower values of Reynolds number. The pressure along the downstream side drops quickly with the rise of surface temperature. A decreasing pressure is found near the rear stagnation point as Ri

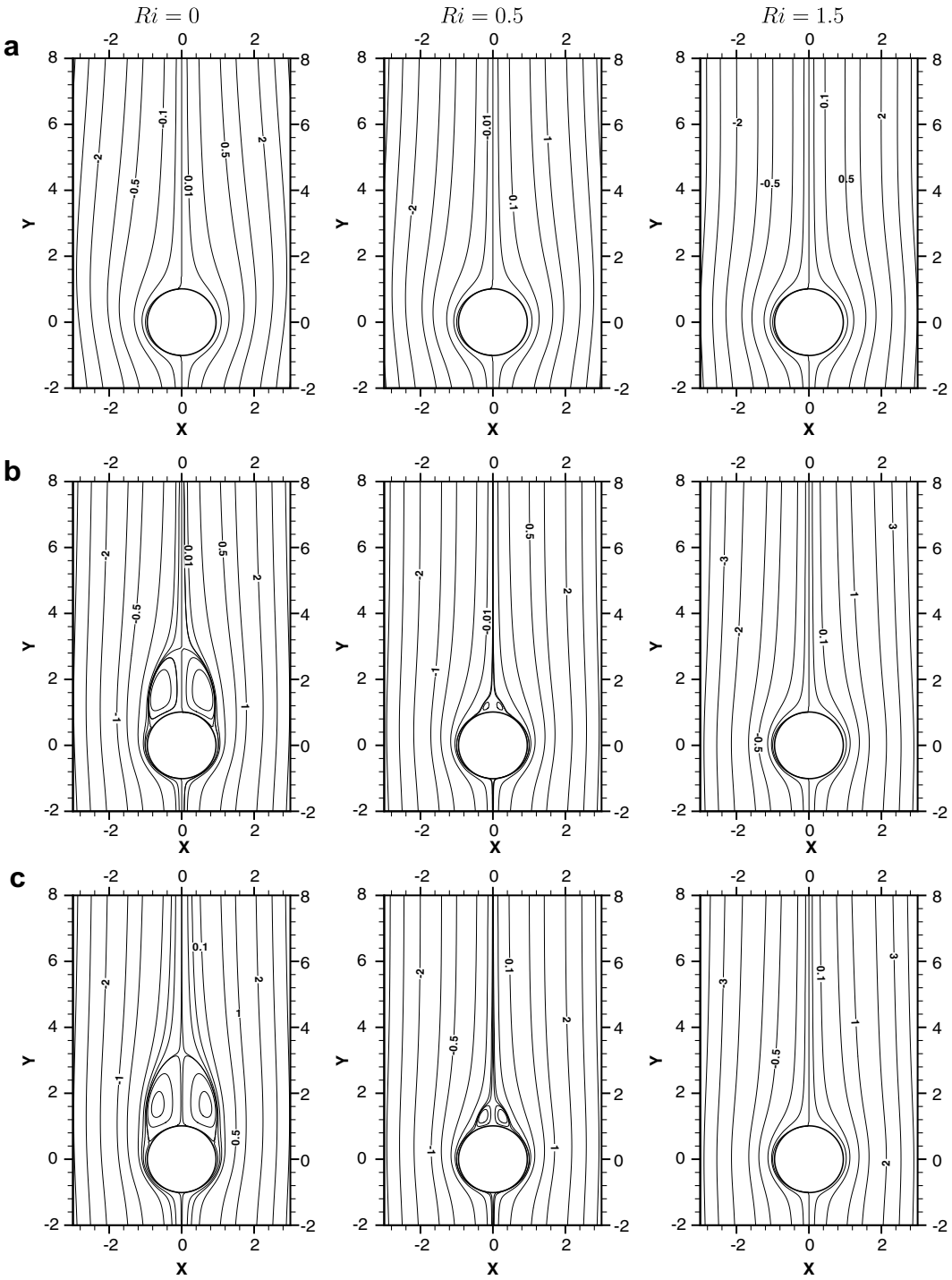

Fig. 8. Stream lines for the axisymmetric flow at different *Ri*. (a) $Re = 1$; (b) $Re = 150$; (c) $Re = 200$.

increases. This drop in surface pressure in the downstream side is associated with the acceleration in boundary layer through surface heating. At $Ri = 0$, the adverse pressure gradient is strong enough to cause the flow separation. At $Ri = 0.5$, a smaller zone of adverse gradient near the rear stagnation point ($\theta = 0$) occurs for $Re > 110$. When $Ri = 1.5$ the additional energy supplied by the buoyancy forces enable the fluids to overcome the adverse pressure gradient.

The effect of Reynolds number on the drag coefficient (C_d) experienced by the sphere is presented in Fig. 12a at different values of $Ri = 0, 0.5, 1.5$. The variation of the drag at lower range of Reynolds number, $1 \leqslant Re \leqslant 10$, is shown separately in Fig. 12b. The drag coefficient decreases with the increase of Reynolds number, and the variation in drag coefficient with Reynolds number is much faster for lower range of Reynolds number. The drag coefficient depends on the surface pressure distribution and the surface

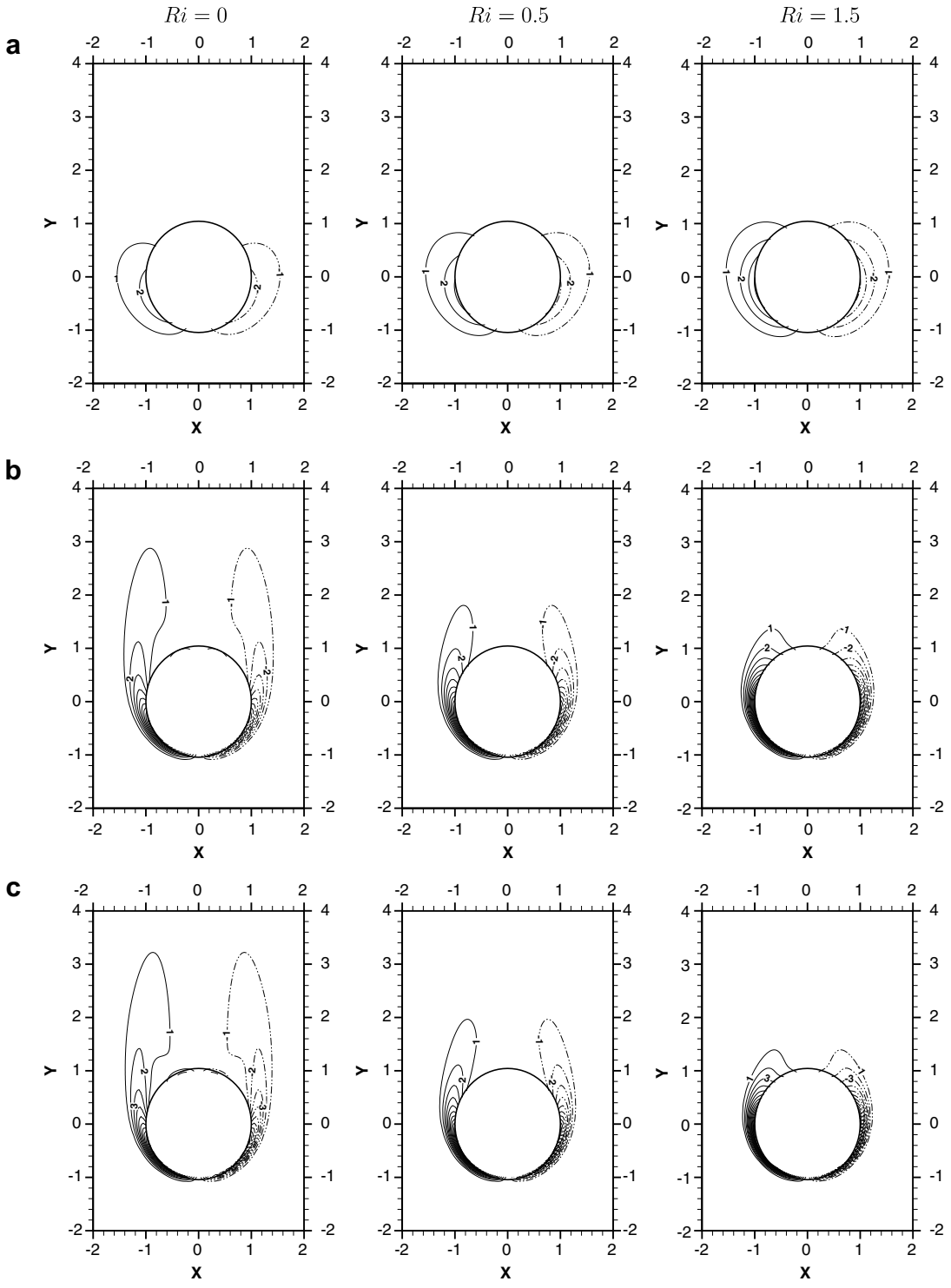

Fig. 9. Vorticity contours for axisymmetric flow at different Ri. (a) $Re = 1$; (b) $Re = 150$; (c) $Re = 200$.

vorticity. The decrease in drag coefficient with increase of Reynolds number is due to the increase of the wake size. For the case of forced convection ($Ri = 0$), Feng and Michaelides [6] proposed an empirical formula for the drag coefficient valid for moderate values of Reynolds number as

$$C_d = 24(1 + Re^{2/3}/6)/Re.$$

Our results are in excellent agreement with this formula for $Re > 10$ (see Fig. 4). However, for $Re < 10$ our results deviate from this formula. At the lower range of Reynolds number, the variation in drag due to the change in surface temperature is much faster compare to the higher Reynolds number case. The increase in Richardson number produces an increment in drag coefficient for the range of Reynolds

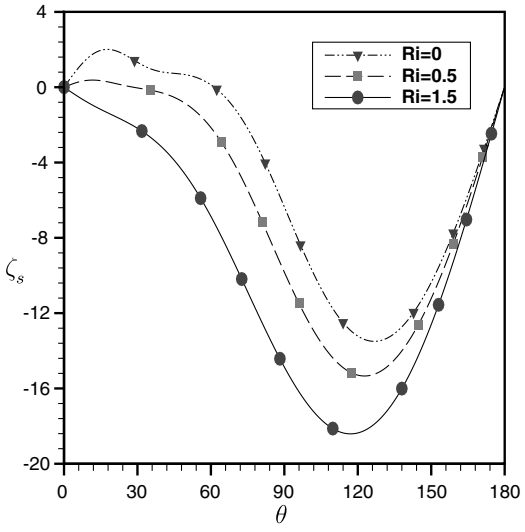

Fig. 10. Surface vorticity distribution (ζ_s) at $Re = 200$ for different Ri ($=0, 0.5, 1.5$).

number considered, i.e., $1 \leqslant Re \leqslant 200$. Increase in Richardson number causes an enhancement in drag coefficient. We have seen before in the vorticity contours that the increase in surface temperature causes a reduction in wake length which results into an increment in drag coefficient.

The angle of flow separation (θ_s) from the surface of the sphere is presented in Fig. 13 for different values of Reynolds number ($20 \leqslant Re \leqslant 200$) and Richardson number ($Ri = 0, 0.25, 0.5$). The separation angle is measured from the forward stagnation point. The separation point moves towards the rear stagnation point with the rise of surface temperature at a fixed Reynolds number. Thus the size of the wake reduces with the rise of surface heat.

The temperature distribution in the wake is shown in Fig. 14 for $Re = 1$, 150 and 200 at $Ri = 0$, 0.5, 1.5. At $Re = 1$ we considered $Gr = 0$ ($Ri = 0$), $Gr = 0.5$ ($Ri = 0.5$) and $Gr = 1.5$ ($Ri = 1.5$). It is clear from the figures that at lower values of Re and Gr the heat transfer is due to conduction and the isotherms form a ring-like structure around the sphere. At higher Reynolds number, the heat transfer is dominated by the convection effect. The maximum crowding of the isotherms is seen in the upstream face of the sphere and the thermal boundary layers grow from the forward stagnation point. The vorticity and temperature are transported into the fluid through a similar type of equation for the case of $Ri = 0$. As the sphere is heated it induces a vertical jet, the downstream eddy collapses at $Re = 150$, and a thermal plume develops in the downstream direction. The plume becomes stronger with the increase of surface heat as well as Reynolds number. At $Ri = 1.5$ and $Re = 150$ the non-dimensional temperature within the plume at a distance $13R$ from the center of the sphere is .3. Our result at $Re = 200$ and $Gr = 6 \times 10^4$ ($Ri = 1.5$) shows that the temperature in the plume at a distance $14R$ from the center of the sphere is not negligible. The thickness of the thermal boundary layer reduces with the increase of Grashof number at a fixed value of Reynolds number. At higher values of Grashof number, the heat leaving the particle is confined to a thin boundary layer and to the plume above the particle in the mixed convection regime ($Ri > 1$). It may be noted that Gan et al. [22] found that the thermal plume, which develops during migration of a hot particle of circular cross-section in a vertical channel, assumes a serpentine shape for higher range of Grashof number. This oscillation in plume, as explained by Gan et al. [22], is due to the presence of vertical wall which creates a lateral pressure gradient. However, the Hu and Patankar [32] study suggests that freely rising thermal plume in ambient air may experience the 'cork-screw' waves. This instability is due to the buckling of the core under the action of the shear stress at the surface of the core [33]. In natural convection over an isothermal sphere, the formation of steady plume at $Gr = 10^8$ has been reported by Yang et al. [19].

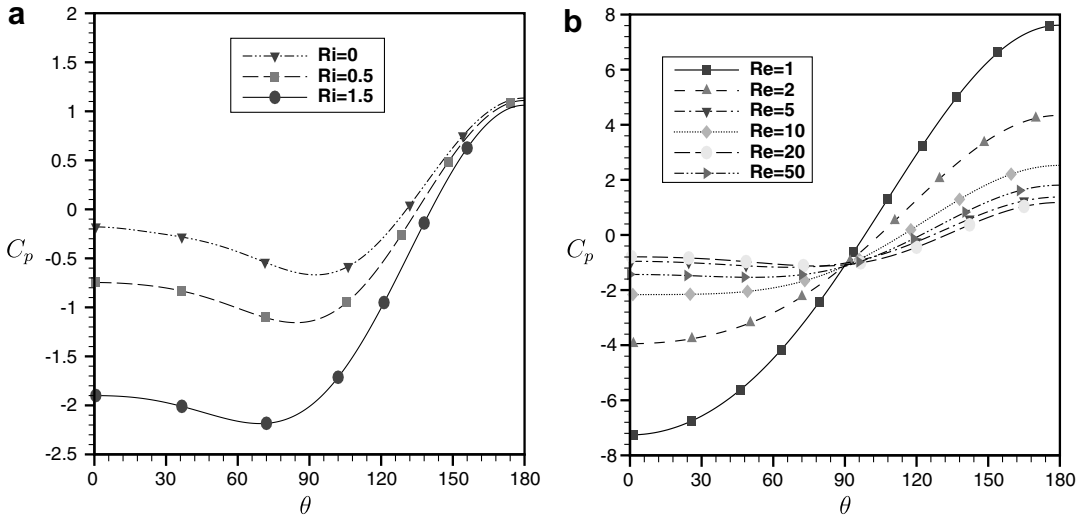

Fig. 11. Surface pressure distribution (C_p) for different values of Re and Ri. (a) $Re = 100$ with $Ri = 0, 0.5, 1.5$; (b) $Ri = 0.5$ with $Re = 1, 2, 5, 10, 20, 50$.

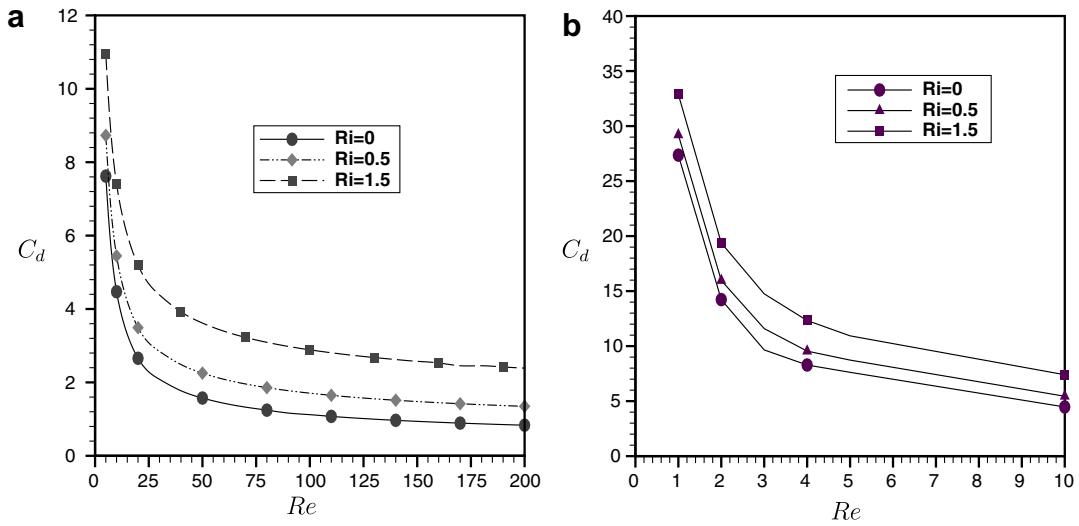

Fig. 12. Effect of Reynolds number varying between 1 and 200 on the drag coefficient (C_d) at different Ri (=0, 0.5, 1.5). (a) $5 \leqslant Re \leqslant 200$; (b) $1 \leqslant Re \leqslant 10$.

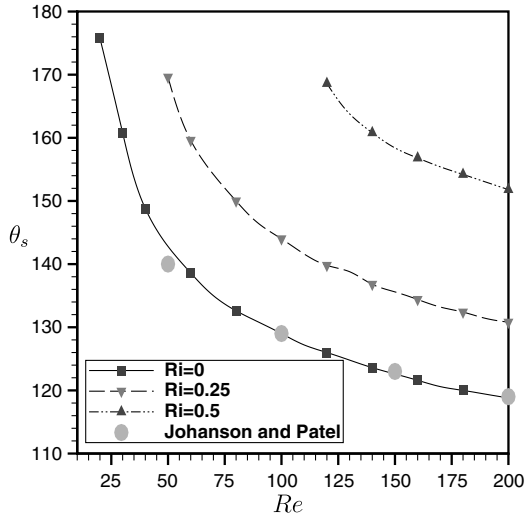

Fig. 13. Effect of Reynolds number ($20 \leqslant Re \leqslant 200$) on the angle of flow separation (θ_s) for different Ri (=0, 0.25, 0.5).

In most applications it is not necessary to know in detail the local temperature field, only the overall heat transfer between the body and fluid needs to be known. The variation of the total Nusselt number with the Reynolds number at different values of Richardson number is presented in Fig. 15a and b. Feng and Michaelides [6] proposed the following correlation for $\overline{Nu}$ for the case of forced convection ($Ri = 0$) with moderate values of Reynolds number as

$$\overline{Nu} = 0.852(PrRe)^{1/3}(1 + 0.233Re^{0.287}) + 1.3 - 0.182Re^{0.355}.$$

Our computed results are in closed agreement with the above formula for $Ri = 0$ (see Fig. 4). For lower range of $Re \leqslant 10$, our computed $\overline{Nu}$ agrees well with the asymptotic solution proposed by Acrivos and Taylor [14]. The rate of heat transfer increases monotonically with the increase of Reynolds number. The influence on $\overline{Nu}$ due to the increment of Richardson number is almost negligible for the lower range of Reynolds number. However, heat transfer increases at a much faster rate with the increase of Richardson number for moderate values of Reynolds number, i.e., $Re \geqslant 50$ (see Fig. 17a). At higher values of Reynolds number, heat transfer is due to convection.

The majority of the study on heated spheres applicable to analyze the particle-droplet systems in air or liquid is considered for the lower range of Reynolds number and Grashof number. The Reynolds number based on micro-to millimeter-sized particles and the settling velocity could be of order one and likewise the Grashof number in the case of air is also of the order one. We computed results to study the buoyancy effect at lower range of Reynolds number. Fig. 16a and b shows the total Nusselt number and drag coefficient when $Re = 1$, 5 and 10 for $0 \leqslant Ri \leqslant 1.5$. The drag coefficient at low Reynolds number, which is mainly due to the viscous force, is enhanced with the increase of Ri. Based on the weak interaction between free and forced convection Mograbi and Bar-Ziv [26,27] proposed an empirical expression for the hydrodynamic drag on a sphere at low range of Reynolds number and Grashof number. They compared the empirical formula with the numerical result for $Gr = 10^{-2}$ and 10^{-4} with $0 \leqslant Ri \leqslant 1$ and found a large discrepancy when Ri is O(1) at $Gr = 10^{-2}$. Our results for drag coefficient for $Re \geqslant 1$, presented in Fig. 16b, does not follow the empirical formula due to Mograbi and Bar-Ziv [26,27]. Thus, for the range of Gr considered in this paper a weak non-linearity assumption for the mixed convection flow is not valid. Increase in Reynolds number produces a large increment in the average rate of heat transfer. The heat transfer remains almost invariant due to the change of Ri at this range of Reynolds number. At lower Reynolds

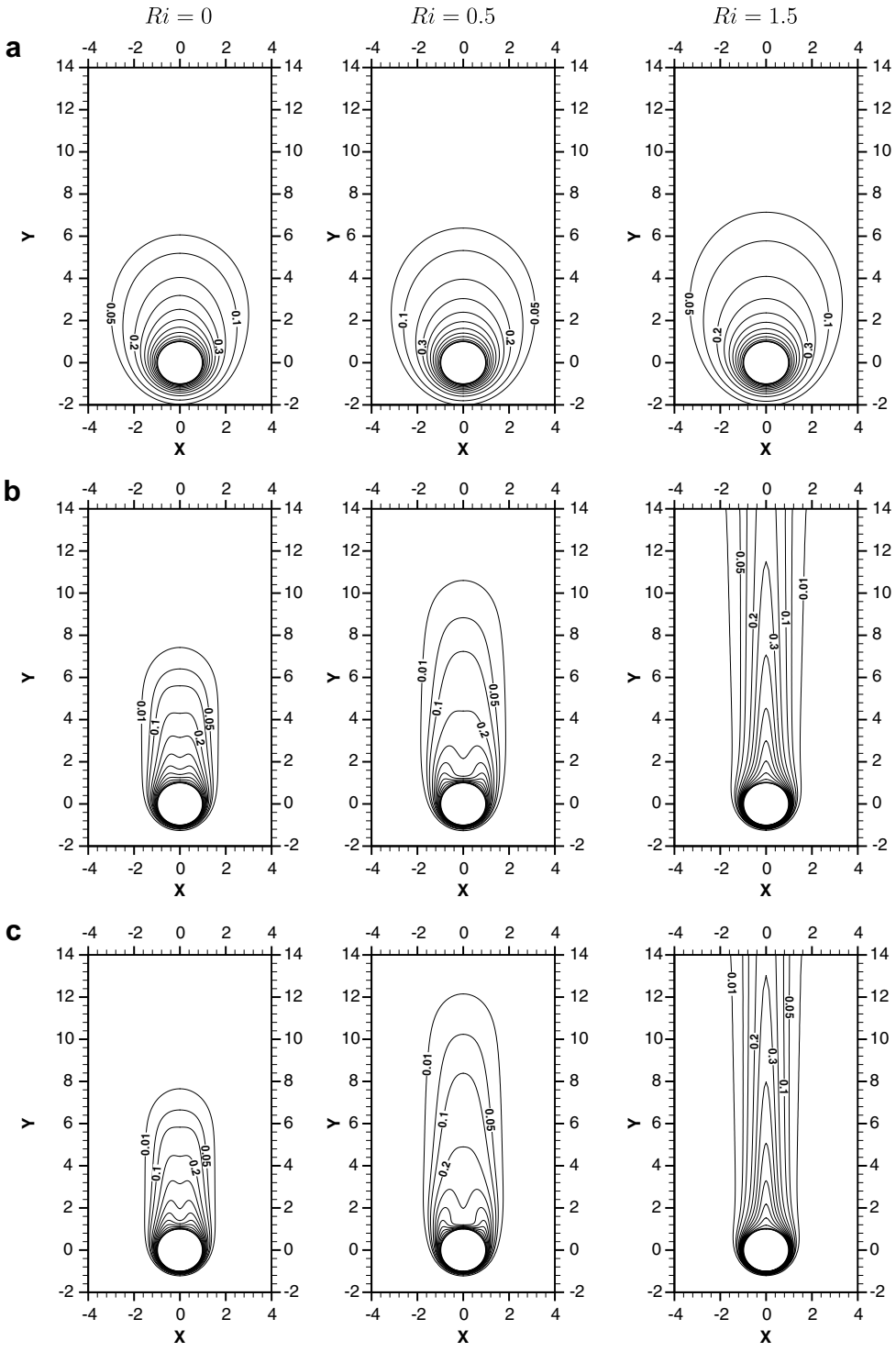

Fig. 14. Isothermal contours for the axisymmetric flow at different Ri (=0, 0.5, 1.5). (a) $Re = 1$; (b) $Re = 150$; (c) $Re = 200$.

number the heat transfer is due to conduction, and it is equal to 2 when Stokes flow is considered ($Re < 1$). An increment in Ri from 0 to 1.5 in the lower range of Re implies a small change in the Grashof number. Thus the trend in $\overline{Nu}$ at lower values of Re in Fig. 16a is justified.

At the moderate values of Reynolds number ($Re = 50, 150, 200$) the variation of total Nusselt number and the drag coefficient is presented in Fig. 17a and b. The drag coefficient increases monotonically with the rise of surface temperature. This is in contrast with the case of natural convection (Fig. 5), where the drag coefficient reduces with the increase of Grashof number. For the case of natural convection the increase in Grashof number reduces the pressure drag. The average rate of heat transfer

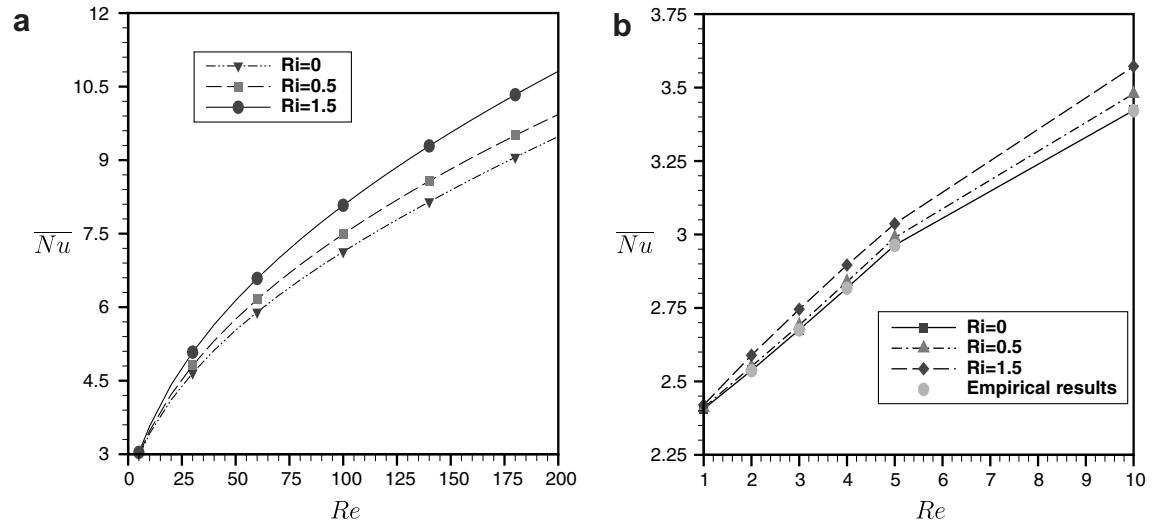

Fig. 15. Effect of Reynolds number ($1 \leqslant Re \leqslant 200$) on the total Nusselt number ($\overline{Nu}$) at different Ri (=0, 0.5, 1.5). (a) $5 \leqslant Re \leqslant 200$; (b) $1 \leqslant Re \leqslant 10$.

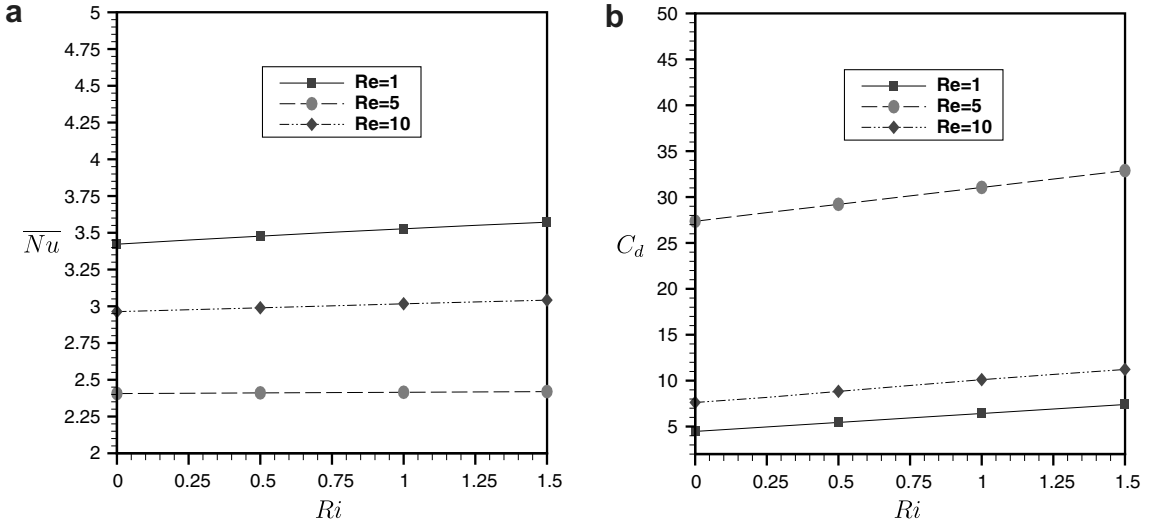

Fig. 16. Effect of Ri on total Nusselt number and drag coefficient at lower values of Re (=1, 5, 10). (a) $\overline{Nu}$; (b) C_d.

increases monotonically with the increase of Grashof number and Reynolds number. Comparing the results for natural convection i.e., Fig. 5. We find that at higher Re ($\geqslant 20$) the rate of increment in total Nusselt number with the increase of Grashof number is found to be lower than the corresponding rate of increment for the natural convection case. This is due to the presence of the recirculating zone in the mixed convection case. Our results show how that both drag coefficient and total Nusselt number varies almost linearly with Grashof number. But the rate of the linear variation is higher at higher Reynolds number for the $\overline{Nu}$.

The steady state Nusselt number for conjugate heat transfer problem when $\phi_\alpha = 1$ have been proposed by several authors as [34]

$$Nu_{\text{conj}} = \left(\frac{1}{\phi_\kappa Nu_{\text{int}}} + \frac{1}{Nu_{\text{ext}}}\right)^{-1} \tag{11}$$

with Nu_{int} and Nu_{ext} are respectively, the Nusselt number corresponding to internal and external problems. It may be noted that for the case of pure diffusion $Nu_{\text{int}} = 6.58$ and the asymptotic expression for Nu_{ext} is $Nu_{\text{ext}} = 1 + [1 + Pe^{-1}]Pe^{0.333}Re^{0.08}$. We have made a comparison of our computed Nu_{conj} with the asymptotic solution at different Re in Fig. 18a. A good quantitative agreement of our computed solution with the asymptotic result given by Eq. (11) is observed for all Reynolds number considered. In Fig. 18b, we present the computed Nu_{conj} and its asymptotic values at different ϕ_κ for $Re = 20$. We also made a comparison of our results with the computed results due

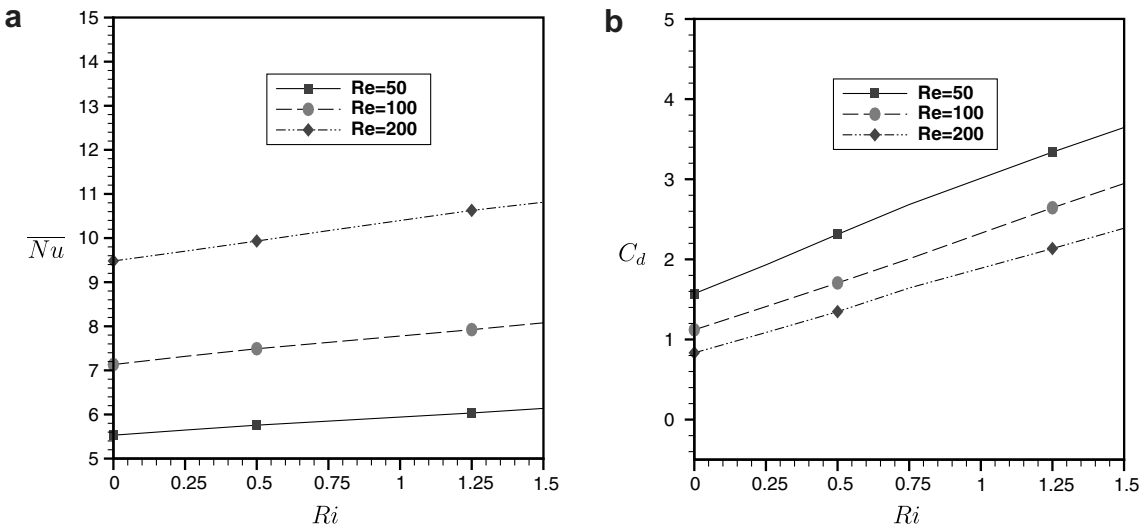

Fig. 17. Effect of Ri on total Nusselt number and drag coefficient at moderate values of Re (=50, 100, 200). (a) $\overline{Nu}$; (b) C_d.

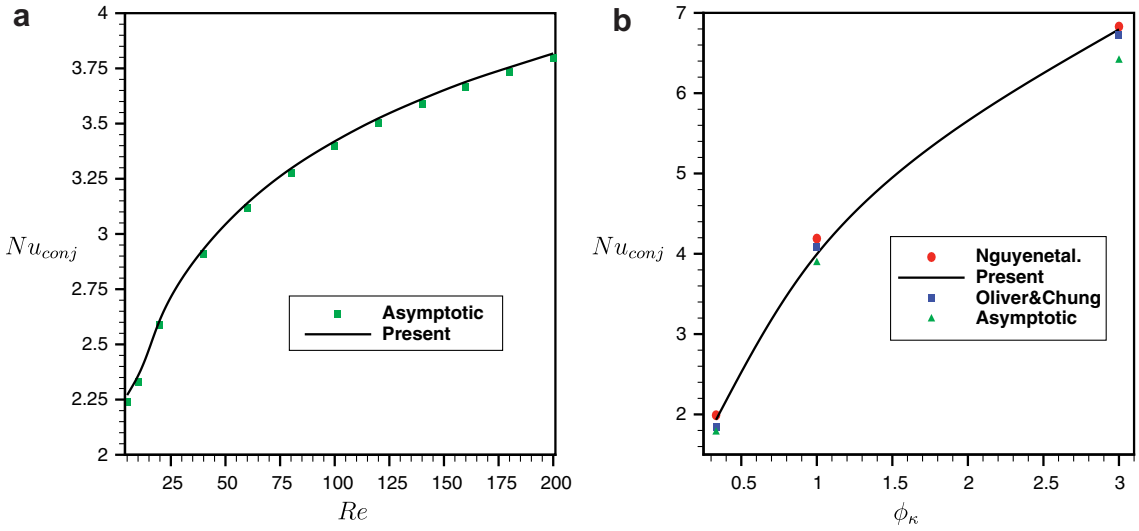

Fig. 18. Computed and asymptotic solution of Nusselt number, Nu_{conj}, for the conjugate heat transfer case when $Gr = 0$ and $\phi_\alpha = 1$. (a) Nu_{conj} at various Re with $Pr = 0.7$ and $\phi_\kappa = 1$; (b) comparison of Nu_{conj} at different values of ϕ_κ with the results due to Oliver and Chung [34], Nguyen et al. [23] and asymptotic solution when $Pe = 300$ and $Re = 20$.

to Nugyen et al. [23] and Oliver and Chung [34] and found them in agreement.

5. Conclusions

In the present study the effects of Reynolds number ($1 \leqslant Re \leqslant 200$) and the Richardson number ($0 \leqslant Ri \leqslant 1.5$) on the buoyancy aided mixed convection around a hot spherical particle falling in air is made. The present analysis presents a clear picture of the mixed convection for low to moderate values of Reynolds number. Our computed solutions for forced convection case ($Ri = 0$) are in close agreement with the empirical/analytical solutions proposed by Acrivos and Taylor [14] and Feng and Michaelides [6]. We have also obtained the Nusselt number for the conjugate heat transfer problem and found them in close agreement with the asymptotic solution obtained by other authors. The main results of this study may be highlighted as follows:

1. For $Re \geqslant 20$ the flow separates and forms a recirculation zone along the downstream. With the rise of sphere surface temperature, the separation point slides towards the rear stagnation point and eventually the vortex collapses to develop a buoyant plume over the sphere. The strength of the plume enhances with the rise of surface temperature. The development of the upward jet from the sphere enhances the drag coefficient and the rate of heat transfer.

2. At lower values of Reynolds number the heat transfer is mostly due to conduction. For moderate values of Reynolds number, the heat transfer is mainly due to convection. Increment in Reynolds number produces an increment in $\overline{Nu}$ for all value of Richardson number.
3. The drag coefficient as well as the heat transfer increases monotonically with the increase of surface temperature for moderate values of Reynolds number. Increase in Re at a fixed Gr increases the wake length and hence produces a reduction in the drag coefficient.
4. Both C_d and $\overline{Nu}$ varies almost linearly with the Grashof number for a fixed value of Re. The rate of increment in C_d with Ri is much higher at lower range of Re.

Acknowledgements

The authors acknowledge the financial support received from the Department of Science and Technology, Govt. of India through a project grant. S. Bhattacharyya gratefully acknowledge the Guest Scientist grant received from the Max Planck Institute for Marine Microbiology, Bremen, Germany during preparation of the manuscript.

References

[1] J. Happel, H. Brenner, Low Reynolds Number Hydrodynamics, second ed., Leiden Noorthdh off International Publishing, 1965.
[2] R. Clift, J.R. Grace, M.E. Weber, Bubbles Drops and Particles, Academic, 1978.
[3] E.E. Michaelides, Particles, bubbles: their motion, Heat Mass Transfer (2006).
[4] N. Patankar, D.D. Joseph, Modeling and numerical simulation of particulate flows by the Eulerian Lagrangian approach, Int. J. Multiphase Flow 27 (2001) 1659–1684.
[5] C. Veeramani, P.D. Minev, K. Nandakumar, A fictitious domain formulation for flows with rigid particles: a non-Lagrange multiplier version, J. Comput. Phys. 224 (2007) 867–879.
[6] Z.G. Feng, E.E. Michaelides, The immersed boundary-lattice Boltzmann method for solving fluid-particles interaction problems, J. Comput. Phys. 195 (2004) 602–628.
[7] R.H. Magarvey, R.L. Bishop, Transition ranges for three-dimensional wakes, Can. J. Phys. 39 (1961) 1418–1422.
[8] T.A. Johnson, V.C. Patel, Flow past a sphere up to a Reynolds number of 300, J. Fluid Mech. 378 (1999) 19–70.
[9] A.G. Tomboulides, S.A. Orszag, Numerical investigation of transitional and weak turbulent flow past a sphere, J. Fluid Mech. 416 (2000) 45–73.
[10] M.C. Thomson, T. Leweke, M. Provansal, Kinematics and dynamics of sphere wake transition, J. Fluids Struct. 15 (2001) 575–585.
[11] R. Natarajan, A. Acrivos, The instability of the steady flow past spheres and disks, J. Fluid Mech. 254 (1993) 323–344.
[12] P. Bagchi, M.Y. Ha, S. Balachandar, Direct numerical simulation of flow and heat transfer from a sphere in uniform cross-flow, J. Fluids Eng. 123 (2001) 347–358.
[13] G. Yun, D. Kim, H. Choi, Vortical structures behind a sphere at subcritical Reynolds numbers, Int. Phys. Fluids 18 (2006) 015–102.
[14] A. Acrivos, T.D. Taylor, Heat and mass transfer from single sphere in stokes flows, Phys. Fluids 5 (1962) 387–394.
[15] H. Brenner, Forced convection heat and mass transfer at small Peclet numbers from a particle of arbitrary shape, Chem. Eng. Sci. 18 (1963) 109–115.
[16] S.C.R. Dennis, J.D.A. Walker, J.D. Hudson, Heat transfer from a sphere at low Reynolds numbers, J. Fluid Mech. 60 (1973) 273–283.
[17] Z.G. Feng, E.E. Michaelides, Heat and mass transfer coefficients of viscous sphere, Int. J. Heat Mass Transfer 44 (2001) 4445–4454.
[18] H. Jia, G. Gogos, Laminar natural convection heat transfer from isothermal spheres, Int. J. Heat Mass Transfer 39 (1996) 1603–1615.
[19] S. Yang, V. Raghavan, G. Gogs, Numerical study of transient laminar natural convection over an isothermal sphere, Int. J. Heat Fluid Flow 28 (2007) 821–837.
[20] D.S. Riley, G.D. Drake, Mixed convection in an axisymmetric buoyant plume, Quart. J. Mech. Appl. Math. 36 (1984) 43–54.
[21] D.S. Riley, M. Tveitereid, On the stability of an axisymmetric plume in a uniform stream, J. Fluid Mech. 142 (1984) 171–186.
[22] H. Gan, J. Chang, J. Feng, H.H. Hu, Direct numerical simulation of the sedimentation of solid particles with thermal convection, J. Fluid Mech. 481 (2003) 385–411.
[23] H.D. Nguyen, S. Paik, J.N. Chung, Unsteady mixed convection heat transfer from a solid sphere: the conjugate problem, Int. J. Heat Mass Transfer 36 (1993) 4443–4453.
[24] G. Ziskind, B. Zhao, D. Katoshevski, E. Bar-Ziv, Experimental study of mixed convection from a heated sphere at small Reynolds and Grashof numbers, cross flow, Int. J. Heat Mass Transfer 44 (2001) 4381–4389.
[25] E. Mograbi, G. Ziskind, D. Katoshevski, E. Bar-Ziv, Experimental study of the forces associated with mixed convection from a heated sphere at small Reynolds and Grashof numbers—part II: assisting and opposing flows, Int. J. Heat Mass Transfer 45 (2002) 2423–2430.
[26] E. Mograbi, E. Bar-Ziv, Dynamics of a spherical particle in mixed convection flow field, J. Aerosol Sci. 36 (2005) 387–409.
[27] E. Mograbi, E. Bar-Ziv, On the mixed convection hydrodynamic force on a sphere, J. Aerosol Sci. 36 (2005) 1177–1181.
[28] K. Hatanaka, M. Kawahara, A numerical study of vortex shedding around a heated/cooled circular cylinder by the three-step Taylor–Galerkin method, Int. J. Numer. Methods Fluids 21 (1995) 857–867.
[29] A. Wang, Z. Travnicek, K. Chia, On the relationship of effective Reynolds number and Strouhal number for the laminar vortex shedding of a heated cylinder, Phys. Fluids 12 (2000) 1401–1410.
[30] J. Chang, M.R. Maxey, Unsteady flow about a sphere at low to moderate Reynolds number: part 1. Oscillatory motion, J. Fluid Mech. 277 (1994) 347–379.
[31] C.R. Torres, H. Hanazaki, J. Ochoa, J. Castillo, W. Van Woert, Flow past a sphere moving vertically in a stratified diffusive fluid, J. Fluid Mech. 417 (2000) 211–236.
[32] H.H. Hu, N. Patankar, Non-axisymmetric instability of core-annular flow, J. Fluid Mech. 290 (1995) 213–224.
[33] R. Bai, K. Chen, D.D. Joseph, Lubricated pipelining: stability of core-annular flow: part 5. Experiments and comparison with theory, J. Fluid Mech. 240 (1992) 97–132.
[34] D.L.R. Oliver, J.N. Chung, Unsteady conjugate heat transfer from a translating fluid sphere at moderate Reynolds numbers, Int. J. Heat Mass Transfer 33 (1990) 401–408.